



Contents lists available at ScienceDirect

Arabian Journal of Chemistry

journal homepage: www.ksu.edu.sa

Original article

Syntheses, properties and mechanistic studies of 8-aminooctanoic acid-modified polyaspartic acid polymers for calcium scale inhibition

Linlin Zhao^{a,c}, Fei Wang^b, Xiaojuan Zhang^a, Yu Han^a, Yuxia Wang^a, Zhenli Yang^c, Zhongyan Cao^{a,*}, Yufeng Wu^{a,*}, Ying Xu^{a,*}^a College of Chemistry and Molecular Sciences Henan University, Kaifeng 475004 China^b Zhengzhou Dongxing Environmental Energy Co., Ltd., Zhengzhou 451450 China^c Henan Chemical Technicna College, Kaifeng 475004 China

ARTICLE INFO

Keywords:

Polyaspartic acid
8-Aminooctanoic acid
Scale inhibition
Mechanism

ABSTRACT

The anti-scaling agent poly(aspartic acid) (PASP) polymers had become a hot research topic based on its peptide bond structures with degradation characteristics. However, it was difficult to control the chain length distributions of the synthesized products, which led to difficulty in determining the scaling mechanism for the peptide bond products. In this paper, PASP/8AC graft modified polymers with a narrow dispersity (\mathcal{D}) and controllable chain lengths was synthesized via a simple two-step method, and 8-aminooctanoic acid (8AC) was introduced into the peptide bond structure of PASP with main chain lengths of 12. The effects of the side-chain lengths and functional groups on the scale inhibition mechanism were determined. The static scale inhibition results showed that the grafted products had significantly improved scale inhibition efficiencies at low concentrations and good temperature and time stabilities. The inhibition rate for CaSO_4 scaling was increased by almost 60 % at a concentration of 3 mg/L. At 5 mg/L, the inhibition rate for CaCO_3 scaling was increased by 36 %. X-ray photoelectron spectroscopy (XPS) and density functional theory (DFT) showed that side chain length extensions improved calcium ion chelation by the PASP and increased calcium scale lattice distortion. This study verified the effects of side chains on PASP scale inhibition and its mechanism. This is of great importance in designing new green water treatment agents.

1. Introduction

In industrial production processes, physical and chemical methods are usually used to reduce the safety risks and economic losses due to scaling by the circulating cooling water, corrosion of pipelines, microbial growth, etc (Lin et al., 2020, Piyadasa et al., 2017). Due to their economic efficiencies, chemical methods are favored in industry. Chemical methods usually involve adding chemicals to control water quality parameters such as the pH and dissolved oxygen level (Khormali et al., 2018, Jafar Mazumder et al. 2020). The addition of scale and corrosion inhibitors is currently the most widely used and most promising method.

The common commercial scale and corrosion inhibitors are phosphates, phosphonates, polymethacrylic acids, polysulfonic acids, polycarboxylic acids and their derivatives, which are inexpensive and highly effective (Yan et al., 2020, Du et al., 2018). However, phosphorus-containing scale inhibitors tend to cause water eutrophication, so their

use has been limited (Glibert et al. 2017). Polysulfonic acids and polycarboxylic acids are nonphosphorus-scale inhibitors and exhibit high scale inhibition efficiencies and dispersion but poor biodegradation performance (Wallace et al., 2013, Ji et al., 2017). In recent years, green corrosion and scale inhibitors have been developed to respond to environmental protection policies (Ansari et al., 2023, Eichinger et al., 2022, Zhang et al. 2018). Polyglutamic and polyaspartic acid have become the focus of research because of their excellent resistance to calcium carbonate scale, nontoxicity and good biodegradability (Syeda et al., 2023, Zhang et al., 2017, Zhao et al., 2022). At present, the literature describes the use of PASP as a water treatment agent (Cai et al., 2022, Zeino et al., 2018). To further corrosion inhibition, calcium sulfate scale inhibition and calcium phosphate properties, many functional groups were introduced to provide polyaspartic acid derivatives, such as PASPTU, Arg-SA-PASP, and PASP/ASA (Zhang et al. 2018, Chen et al., 2020, Zhao et al., 2021). Some polar functional groups, such as COOH , OH , NH_2 , and SO_3H , were shown to play active roles in scale inhibition, dispersion and

* Corresponding authors.

E-mail addresses: zycao@henu.edu.cn (Z. Cao), wuyufeng@henu.edu.cn (Y. Wu), hdcxuxu@126.com (Y. Xu).<https://doi.org/10.1016/j.arabjc.2024.105717>

Received 24 November 2023; Accepted 6 March 2024

Available online 7 March 2024

1878-5352/© 2024 The Author(s). Published by Elsevier B.V. on behalf of King Saud University. This is an open access article under the CC BY-NC-ND license (<http://creativecommons.org/licenses/by-nc-nd/4.0/>).

corrosion inhibition (Li et al., 2023, Qiang et al., 2021, Rbaa et al., 2020). Complexation solubilization, lattice distortion, ion exchange, etc., are also recognized as the mechanisms for water treatment agents (Wang et al., 2023, Liu et al. 2020). Nevertheless, direct evidence on the mechanism of action for water treatment agents is still scarce.

It's worth noting that scale and corrosion inhibition properties are significantly affected by the molecular weight (Xiang et al., 2018, Whitfield et al., 2021). In particular, the distribution range for the molecular weight and the type of modification groups in the polymer play decisive roles in the corrosion and scale inhibition performance (Li et al., 2021, Liu et al., 2023). However, the precise synthetic conditions required to determine the molecular weight distributions of polymer products and small molecule modifications are difficult to control, which hinders research and development efficiency and the use in polymer water treatment. (Wang et al., 2003, Nomura et al. 2005, Ali et al., 2015). In addition, the methods and mechanisms for corrosion inhibition and scale inhibition are fuzzy and superficial due to the lack of a convincing and detailed scientific basis. The research and development of new high-efficiency water treatment agents has been seriously hindered. Accordingly, there is an urgent need to explore the precise synthesis conditions for the polymers and the anti-scale and corrosion pathways and mechanisms of the related functional groups, which have important potential significance.

To reveal the scale inhibition mechanism of the green water treatment agent based on the previous work of our group, 8-aminooctanoic acid-modified polyaspartic acid polymers (PASP/8AC) were prepared via a molecular weight-controlled reaction. The structure was characterized by Fourier transform infrared (FTIR) spectroscopy, gel permeation chromatography (GPC) and nuclear magnetic resonance spectrometry (NMR). The morphology and processes of calcium carbonate and calcium sulfate scale formation in the absence and presence of PASP/8AC at suitable concentrations were analyzed with the static scale inhibition method, scanning electronic microscopy/X-ray diffraction (SEM/XRD), and X-ray photoelectron spectroscopy (XPS). Finally, the mechanism of the PASP/8AC scale inhibitor was analyzed at the molecular and atomic levels with density functional theory (DFT).

2. Experimental

2.1. Reagents and instruments

β -Benzyl-L-aspartate *N*-carboxy-anhydride (BLA-NCA) was purchased from Adamas Chemical Reagent Co. Ltd. (Shanghai, China). 8-Aminooctanoic acid (8AC), tetrahydrofuran (THF), *N,N*-dimethylformamide (DMF), NaOH and NaHCO₃ were purchased from Tianjin De'en Chemical Reagents Co. Ltd. (Tianjin, China). Anhydrous sodium sulfate, sodium carbonate and potassium hydroxide were purchased from Tianjin Komi Chemical Reagent Co. Ltd. (Tianjin, China). Dichloromethane, anhydrous borax, calcium chloride, potassium chloride and sodium chloride were purchased from Shanghai Shaoyuan Chemical Reagent Co. Ltd. (Shanghai, China). Ethylenediaminetetraacetic acid disodium salt dihydrate (EDTA) was provided by Shanghai Energy Chemical Reagent Co. Ltd. (Shanghai, China). Absolute ethanol was provided by Anhui Ante Food Co. Ltd. (Anhui, China). Hydrochloric acid (36%) was provided by China Pingmei Shenma Group Kaifeng Dongda Chemical Co. Ltd. (Kaifeng, China). Deionized water (DI) was prepared in the laboratory and used for rinsing.

The instruments used in this paper included an HH-601 constant-temperature water tank (China), a VERTEX 70 Fourier transform infrared spectrometer (Germany), an AVANCE 400 nuclear magnetic resonance spectrometer (Germany), an ESCALAB 250Xi X-ray photoelectron spectrometer (UK), a JSM-7610F SEM (Japan), a Nano ZS particle size and zeta potential analyzer (England), a D8 Advance X-ray powder diffractometer (Germany), and a TDAmx gel permeation chromatography (UK).

2.2. Synthesis of PASP/8AC

Based on ring-opening polymerization of α -amino acid-*n*-carboxylic acid anhydride (NCA) for the preparation of polypeptide polymers, following the controllable polymer synthetic method of Cao et al. (Zhang et al., 2024), the PASP/8AC polymer was synthesized by ring-opening polymerization of NCA by optimizing the reaction conditions (Nakanishi et al., 2007, Uchida et al., 2011). The synthetic route to the PASP/8AC scale inhibitor is shown in Fig. 1. The detailed steps are described below.

PASP was prepared by conventional ammonia-induced NCA-controlled polymerization. A mixture containing BLA-NCA (2.0 mmol) and DMF (1 mL) in a Schlenk flask was diluted with 10 mL of CH₂Cl₂. 8-Aminooctanoic acid (0.30 mmol) was then added to the above solution. The reaction was stirred under a dry argon atmosphere at 35 °C for 72h. The lower organic phase was extracted three times with distilled water and vacuum dried to give the PBLA/8AC product (0.31 g, 54%).

PBLA/8AC (0.09 g, 0.45 mmol) was dissolved in THF (5 mL) with stirring at 0 °C. The mixture containing NaOH (0.016 g, 0.40 mmol) was then added dropwise to the above solution, and the reaction was allowed to continue for 24h. After vacuum drying, the solution was extracted with ethyl acetate and purified with a 500 molecular weight dialysis bag to give PASP/8AC (0.06 g, 78%).

2.3. Characterization of PASP/8AC

The zeta potential of PASP/8AC was measured with a nanoparticle size and zeta potential analyzer (Nano ZS Malvern Instruments Co., Ltd., England). The molecular weight of the prepared PASP/8AC was determined by gel permeation chromatography (PL-GPC50, Agilent, UK). The structure of PASP/8AC was characterized with a VERTEX 70 FTIR spectrometer (Bruker Optics, Germany) and ¹H nuclear magnetic resonance spectrometer (¹H NMR; AVANCE 400 MHz NMR spectrometer, Bruker Optics, Germany).

2.4. Static scale inhibition test

To evaluate CaCO₃ and CaSO₄ scale inhibition by PASP/8AC, a static test was carried out according to the National Standard method (GB/T 16632-2008). For CaCO₃, solutions of scale inhibitor (1 mg/mL), sodium tetraborate decahydrate (0.010 mol/L), CaCl₂ (0.15 mol/L) and NaHCO₃ (0.30 mol/L) were prepared in advance. Then an appropriate volume of distilled water, a certain volume of scale inhibitor, 10 mL of sodium tetraborate decahydrate solution, 10 mL of CaCl₂ solution and 10 mL of NaHCO₃ solution were added successively to the 250 mL Erlenmeyer flask. Finally, the above test solution containing Ca²⁺ (240 mg/L, 6.0 mmol/L) and HCO₃⁻ (732 mg/L, 12 mmol/L) with different concentrations of antiscalants was heated at 80 °C for 10h. Finally, after cooling the above solution to room temperature, 25 mL of filtrate was taken and calibrated with standard EDTA solution (0.010 mol/L) for CaCO₃.

In contrast to calcium carbonate, a CaSO₄ scale inhibitor solution (1 mg/mL) was prepared containing 0.026 mol/L sodium tetraborate decahydrate solution, 0.25 mol/L CaCl₂ solution and 0.50 mol/L Na₂SO₄. Distilled water, scale inhibitor, 25 mL sodium tetraborate decahydrate, 50 mL CaCl₂ and 25 mL Na₂SO₄ were added to a 250 mL Erlenmeyer flask and the above solutions containing Ca²⁺ (2000 mg/L, 50 mmol/L) and SO₄²⁻ (4800 mg/L, 50 mmol/L) and different concentrations of inhibitor were heated at 70 °C for 6 h. The test solution containing Ca²⁺ (2000 mg/l, 50 mmol/l) and SO₄²⁻ (4800 mg/l, 50 mmol/l) and different concentrations of scale inhibitors as described above was heated at 70 °C for 6 h. The relevant experimental methods and calculations were also described in previous work (Cai et al., 2022). The scale inhibition efficiencies (η , %) for CaCO₃ and CaSO₄ were calculated with Formula (1).

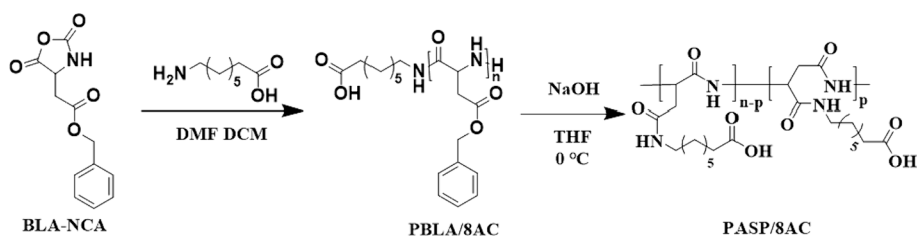


Fig. 1. Synthetic route to PASP/8AC.

$$\eta (\%) = \frac{v_2 - v_1}{v_0 - v_1} \times 100\% \quad (1)$$

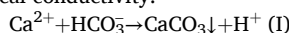
where V_0 is the volume of EDTA consumed before reactions in the absence of the scale inhibitor, mL. V_2 and V_1 are the volumes of EDTA consumed after reactions in the presence and absence of the scale inhibitor, respectively. Each test was repeated three times, and the average data were used to minimize the data scattering.

2.5. XRD, XPS, and SEM analyses

Calcium scale deposition in static scale inhibition experiments was analysed. The surface morphologies of the scale samples used in the static test were observed by field emission scanning electron microscopy (SEM JSM-7610F, Japan). The crystalline form of the calcium scale was investigated with an X-ray powder diffractometer (XRD D8 Advance Bruker, Germany). The Ca 2p binding energies of the calcium scale crystals formed in the presence and absence of the scale inhibitor were analyzed to determine chelation of the scale inhibitor and Ca^{2+} with X-ray photoelectron spectroscopy (XPS ESCALAB 250Xi Thermo Fisher Technologies LTD, UK).

2.6. Induction time for scale formation

The formation process of CaCO_3 is shown in reaction Equation I. To investigate the effect of the inhibitor on scale formation, the pH of the solution was determined. The induction time (t_{ind}) of the CaCO_3 solution was considered to be the point at which the pH of the solution dropped significantly (Stamatakis et al., 2005, Liu et al. 2020), and S are the supersaturation ratios for different solution concentrations. Based on the relationship between t_{ind} and $1/(\ln S)^2$, the t_{ind} of the CaCO_3 crystals was calculated according to the classical homogeneous nucleation theory (Formula 2) (Chien et al., 1999, Giuseppe et al., 2017). Specifically, solutions A, B, C and D, which had different concentrations (0.015, 0.02, 0.025 and 0.03 mol/L, respectively), were obtained by mixing equal molar concentrations of CaCl_2 and NaHCO_3 solutions. The corresponding S values of solutions A, B, C and D were 93.325, 144.524, 204.174 and 269.153, respectively. Then, appropriate amounts of the scale inhibitor were added to the premixed solution. It is worth noting that the solution temperature was kept constant at $25.0 \pm 0.1^\circ\text{C}$. CaCO_3 crystallization released H^+ , resulting in a change in the pH, thus indicating the induction time. The CaSO_4 content was determined by measuring electrical conductivity.



$$\ln t_{ind} = B + \frac{\beta \gamma^3 v_m^2 N_A f(\theta)}{R^3 T^3 (\ln S)^2} \quad (2)$$

where B is the constant, β is a geometrical factor of $16\pi/3$ for spherical nuclei, γ is the surface energy ($\text{J}\cdot\text{m}^{-2}$), v_m is the molar volume of phase formation, N_A is Avogadro's constant (mol^{-1}), $f(\theta)$ is the correction factor, which is equal to 1 for homogeneous nucleation and less than 1 for heterogeneous nucleation, R is the gas constant ($\text{J}\cdot\text{mol}^{-1}\cdot\text{K}^{-1}$), T is the absolute temperature (K). Each value was tested three times, and the average value was cited to minimize data scattering.

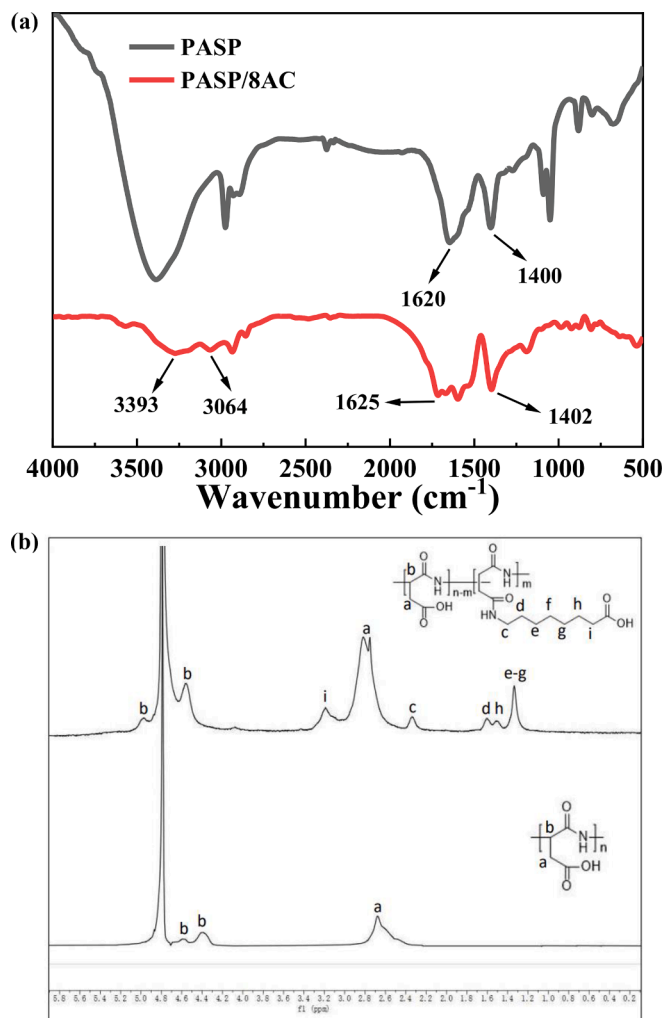
2.7. Scale inhibition mechanism

The molecular structure of PASP/8AC was optimized with the Gaussian 09 software package at the B3LYP/6-31 G level, and scale inhibition by PASP/8AC was analyzed by density functional theory (DFT).

3. Results and discussion

3.1. Chemical characterization of PASP/8AC

The FTIR spectra is shown in Fig. 2a. The FTIR spectra of PASP showed the stretching vibrations of the amide C=O bonds and the absorption peak for the C-N amide stretching vibration at 1620 cm^{-1} and $\sim 1400\text{ cm}^{-1}$, respectively. In addition, the peaks for the C-N stretching

Fig. 2. FTIR spectra (a) and ^1H NMR spectra (b) of PASP and PASP/8AC.

vibration and the N–H bending vibration overlapped. The stretching vibration of the N–H bonds in the PASP amide appeared at 3500 cm^{-1} . The absorption peaks at 2930 cm^{-1} and 2890 cm^{-1} were caused by stretching vibrations of the $-\text{CH}_2-$ and $-\text{CH}-$ groups in the PASP backbone, respectively. In the PASP/8AC FTIR spectra, in addition to the characteristic absorption peaks of PASP, stretching vibration absorption peaks at $\sim 2950\text{ cm}^{-1}$, $\sim 2870\text{ cm}^{-1}$ and $\sim 2850\text{ cm}^{-1}$ were attributed to $-\text{CH}_2\text{CH}_2\text{CH}_2\text{CH}_2\text{CH}_2\text{CH}_2\text{CH}_2-$ in 8-aminooctane acid. Additionally, the peak for the N–H bond in $-\text{CONH}-$ was affected by the branched chain, which reduced the dipole distance. The above evidence indicated that 8-aminocaproic acid participated in the ring-opening reaction and successfully modified the PASP.

Fig. 2b presents the ^1H NMR spectra of PASP and PASP/8AC in D_2O . The signals for the $-\text{CH}-$ and $-\text{CH}_2-$ groups in the PASP main chain were located at 4.3 ppm and 2.6 ppm (with an integrated ratio of 1:2), respectively. The spectra of PASP/8AC showed new signals at $\delta_{\text{H}} = 2.20$ ppm and $\delta_{\text{H}} = 3.10$ ppm that were attributed to the $-\text{CH}_2-$ groups (with an integrated ratio of 1:1) of the side chains in 8-aminooctane acid. In addition, the signals at 1.16 ppm–1.45 ppm were assigned the $-\text{CH}_2\text{CH}_2\text{CH}_2\text{CH}_2\text{CH}_2-$ groups of the 8-aminooctane acid. Unfortunately, since PASP and PASP/8AC were only dissolved in D_2O , the signals for $-\text{COOH}$ and $-\text{NH}-$ were not present due to polarization. Nevertheless, the above results proved the successful synthesis of PASP/8AC.

The molecular weights of PASP and PASP/8AC were measured with the GPC method (Table 1). The weight average molecular weight (M_w) and number average molecular weight (M_n) of PASP/8AC were 13,572 and 11,891 Da, respectively. The dispersity ($D = M_w/M_n$) of PASP/8AC was 1.141. These data indicated that the prepared PASP/8AC had a narrow molecular weight distribution. It has been proven that the molecular weights and molecular weight distributions of polymers have important effects on their properties (Younes et al., 2015; Čožková et al., 2017). Additionally, these reports revealed that overly large or small polymer molecular weights affect scale inhibition, and the appropriate molecular weight is required for the optimal effect (Yan et al., 2020; Cao et al. 2024). Moreover, the zeta potentials of PASP (-4.77 mV) and PASP/8AC (-10.56 mV) were obtained. Both PASP and PASP/8AC scale inhibitors carry a negative charge and can interact electrostatically with positively charged Ca^{2+} ions. Compared with PASP, PASP/8AC with more negative charge can adsorb more positively charged Ca^{2+} ions, thus reducing the deposition of calcium scale. These results indicated that PASP/8AC carried a higher negative charge, which enabled complexation of more Ca^{2+} and inhibit the formation of scale crystals.

3.2. Scale inhibition performance of PASP/8AC

3.2.1. Inhibition of CaCO_3

To investigate the inhibition effect of PASP/8AC on calcium carbonate scale formation, the CaCO_3 inhibition efficiencies of PASP and PASP/8AC were measured with the static scale inhibition method. The relationships among the concentration, temperature and time and reagent resistance to calcium carbonate scaling are shown in Fig. 3. Fig. 3 shows that with increases in the concentration of the agent, the scale inhibition efficiency also increased gradually. When the concentration was 5 mg/L, the scale inhibition efficiency of PASP/8AC reached 42%, while the scale inhibition performance of PASP at the same concentration was only 6% (Fig. 3a). However, the scale inhibition efficiencies of

Table 1

Molecular weights and distribution of the PASP and PASP/8AC grafted copolymer.

Samples	Parameters		
	M_n	M_w	D
PASP	1778	2039	1.147
PASP/8AC	11,891	13,572	1.141

the agents were close to the maximum at 30 mg/L, and those of PASP and PASP/8AC were approximately 47% and 63%, respectively. Nevertheless, the scale inhibition efficiency of PASP/8AC was always better than that of PASP in this concentration range. This may be because, compared with PASP, PASP/8AC contained more $-\text{OH}$ and $-\text{COOH}$ groups, which chelated more Ca^{2+} ions, thus inhibiting the formation and growth of calcium carbonate crystals. When the concentration exceeded 50 mg/L, the scale inhibition efficiency of the agent showed a slight decrease. The inhibitor itself contains a large number of $-\text{COOH}$ and $-\text{OH}$, with increasing concentration, due to the role of van der Waals forces such as H-bonds, resulting in agglomeration between the inhibitor, the effective functional groups are wrapped, the number of functional groups chelating the Ca^{2+} ions in solution is reduced, thus showing a tendency to reduce the scaling inhibition efficiency of the agent.

In addition, the influence of temperature on the scale inhibition efficiencies of the agents with 30 mg/L were also monitored, as shown in Fig. 3b. In the test temperature range, the scale inhibition efficiency of PASP/8AC is higher than that of PASP. At 80°C , the scale inhibition efficiency of PASP/8AC can still reach 63%, which indicates that PASP/8AC has wider temperature range. However, both PASP and PASP/8AC showed decreasing trends in the inhibition efficiency of CaCO_3 scale with increasing temperature. At low temperature, the solubility of calcium scale is relatively low, the number of scale inhibitor molecules is relatively large, and the structure is stretched, the effective functional groups can effectively bind the Ca^{2+} ions in solution, scale inhibition efficiency is high. With the increase in temperature, the solubility of CaCO_3 also gradually increases, the concentration of calcium ions in the solution becomes greater while the concentration of the agent does not change, the adsorption of the agent on the Ca^{2+} reaches saturation, resulting in the dissolved part of the calcium ions combining with the inorganic salts in the water to form a deposit, and ultimately showing a decrease in the scale inhibiting efficiency of the agent.

In order to determine the time validity of the scale inhibition efficiency of PASP/8AC, the trend of the scale inhibition efficiency of PASP/8AC versus the test time was tested at a concentration of 30 mg/L, as shown in Fig. 3c. The inhibition of CaCO_3 by PASP and PASP/8AC was basically stable in the measured time range and the inhibition rate remained close to 62%. This result shows that PASP/8AC has a good time effectiveness on the scale inhibition efficiency of calcium carbonate scale.

3.2.2. Inhibition of CaSO_4

Many studies have shown that PASP had an undesirable effect on CaSO_4 scale, and many researchers have attempted to improve its performance with various modification methods (Nayunigari et al., 2014; Liu et al., 2011). Accordingly, the CaSO_4 scale inhibition efficiencies of PASP and PASP/8AC were also investigated, and the results are exhibited in Fig. 4. Similar to the scale inhibition efficiency curve for CaCO_3 scale, with increases in the concentration of the agents, the CaSO_4 scale inhibition efficiencies also increased. As shown in Fig. 4a, the CaSO_4 scale inhibition efficiency of PASP/8AC reached 90% at 3 mg/L, while the scale inhibition performance of PASP was only 27%. When the concentration was 4 mg/L, the scale inhibition performance of PASP/8AC reached 99%. Compared with PASP, the inhibition efficiency of CaSO_4 scale was increased by nearly 58%. This indicated that PASP/8AC was more likely to be adsorbed on the CaSO_4 crystals to chelate the Ca^{2+} ions and inhibit the formation of sediments.

Fig. 4b presents the relationship between the test temperatures and scale inhibition performance at the optimal dose of 6 mg/L. It is clear from Fig. 4b that PASP/8AC has a wider temperature applicability range than PASP over the test range. When the temperature was below 80°C , similar to the principle of CaCO_3 scale, the agent is more efficient in preventing calcium sulphate scale, basically maintaining more than 99%. However, the scale inhibition efficiency of PASP decreased sharply at temperatures above 70°C . Although the scale inhibition efficiency of

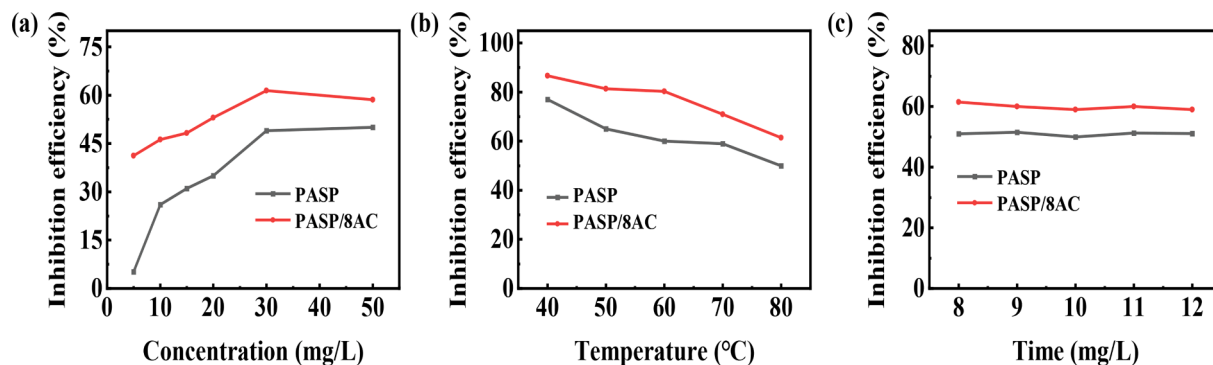


Fig. 3. Inhibition performance of PASP and PASP/8AC against CaCO₃ scaling; (a) concentration, (b) experimental temperature and (c) test time.

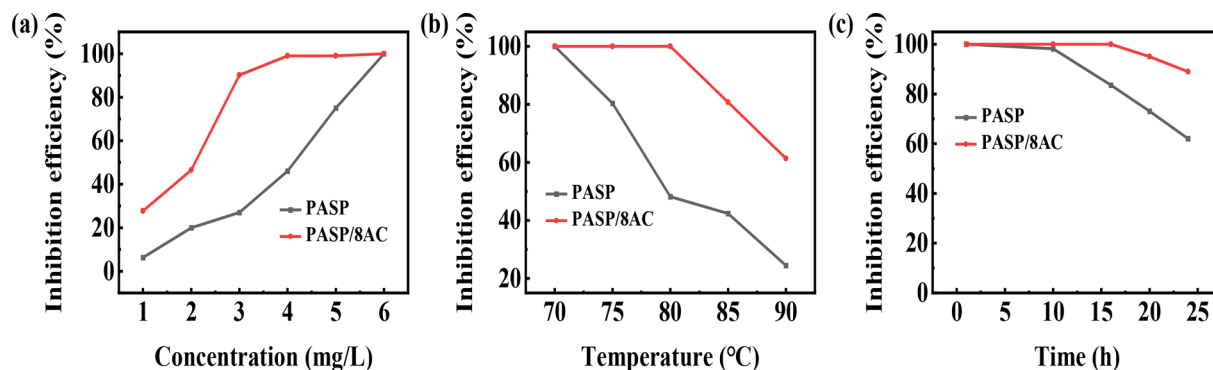


Fig. 4. Inhibition efficiencies of PASP and PASP/8AC against CaSO₄ scale; (a) concentration, (b) experimental temperature and (c) test time.

PASP/8AC also shows a decreasing trend at 80°C, the scale inhibition efficiency is still 52% higher than that of PASP, showing better temperature adaptability. In addition, the relationship between the scale resistance and the test time was also monitored, as shown in Fig. 4c (with the optimal dose of 6 mg/L). In contrast to CaCO₃ scale inhibition, scale inhibition by PASP began to decline when the test time reached 10h. When PASP/8AC was tested for 15h, the scale inhibition efficiency also gradually decreased. The above results showed that compared with PASP, the time-efficiency of PASP/8AC was better than that of PASP because PASP/8AC had branched chains and contained more -COOH groups.

3.3. Surface analyses of CaCO₃ and CaSO₄ scale

3.3.1. Scanning electron microscopy (SEM) characterization

To further reveal the action mechanism of PASP/8AC on calcium scale, the surfaces the CaCO₃ and CaSO₄ scale were analyzed with scanning electron microscopy (SEM) to observe the morphological differences between scales formed without and with the inhibitor. The SEM images of the CaCO₃ scale were obtained without inhibitor addition and in the presence of 10 mg/L and 50 mg/L inhibitor, and the results are displayed in Fig. 5. According to the SEM images, the CaCO₃ scale differed for the sample without added inhibitor (Fig. 5(a)) and the sample with added inhibitor (Fig. 5(b-e)). The morphology of the CaCO₃ flakes shows that in the absence of inhibitors, the calcium carbonate flakes formed have smooth surfaces and regular shapes typical of calcite morphology (Fig. 5(a)). However, after the addition of PASP, the surface

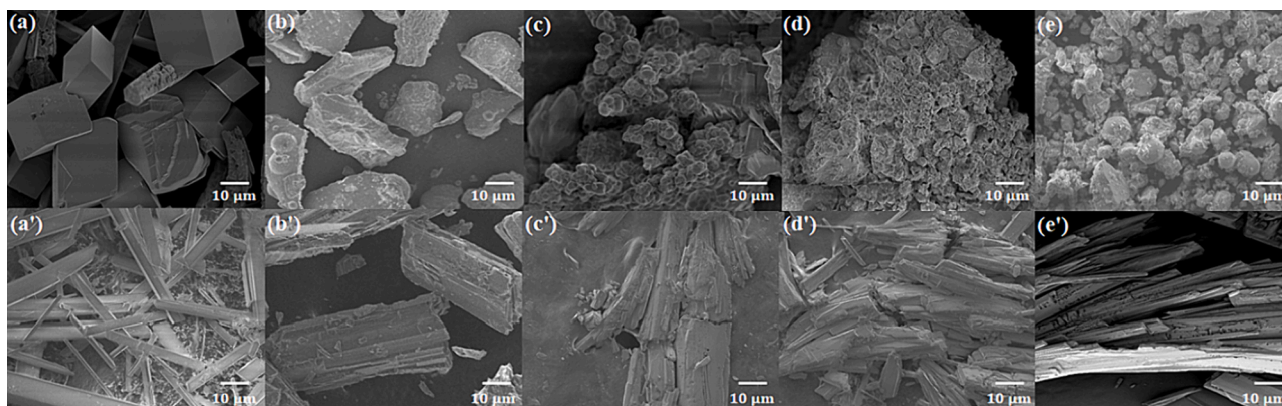


Fig. 5. SEM images of CaCO₃ (a-e) and CaSO₄ crystals (a'-e'); (a) (a') without inhibitor, (b) with 10 mg/L PASP, (c) with 10 mg/L PASP/8AC, (d) with 50 mg/L PASP, (e) with 50 mg/L PASP/8AC. (b') with 1 mg/L PASP, (c') with 1 mg/L PASP/8AC, (d') with 3 mg/L PASP, (e') with 3 mg/L PASP/8AC.

morphology of the CaCO_3 scales was significantly changed, showing fish-scale-like, rough and loose, and the typical calcite morphology was destroyed (Fig. 5(b, d)). With the addition of PASP/8AC, the structure of the CaCO_3 scales was severely damaged and the regular cubes became spherical or fusiform particles, i.e. spherical aragonite morphology (Fig. 5(c, e)). Aragonite is the most unstable crystalline form of CaCO_3 flakes. Because of the long side chains, the PASP/AC polymer easily curled and intertwined and then formed a curved structure. Moreover, the surface contained many polar groups, which induced Ca^{2+} crystallization and finally led to formation of the spheroidal crystals. Herein, the CaCO_3 scale inhibition capacity of PASP/AC was stronger than that of PASP.

In addition, SEM was also used to observe the surface morphologies of the CaSO_4 scale in the absence and presence of the inhibitor, and the results are shown in Fig. 5. The CaSO_4 formed colorless and transparent needle-like or prismatic crystals in the absence of inhibitors (Fig. 5(a')). After the addition of 1 mg/L inhibitors, the surfaces of the CaSO_4 crystal became rougher, replacing the previously smooth forms, and the regular CaSO_4 crystals were destroyed, especially with the addition of PASP/8AC (Fig. 5(c')). When the PASP concentration was increased to 3 mg/L, the previously smooth needle-like CaSO_4 crystals were transformed into a layered, dispersed form (Fig. 5(d')). Nevertheless, the presence of 3 mg/L PASP/8AC directly caused the crystals of CaSO_4 to be sharp, finely fragmented and dispersed, similar to flocculation (Fig. 5(e')). The PASP/8AC graft polymer increased the length of PASP side chains with carboxylic groups through the introduction of 8-aminooctanoic acid. Compared with PASP, the extended side chain of PASP with $-\text{COOH}$ functional group damaged the formation of CaSO_4 crystals more severely, indicating that the extended side chain of PASP effectively participated in the formation of CaSO_4 scale, thus destroying the original morphology of CaSO_4 crystals, and the introduction of 8-aminooctanoic acid further improved the scale inhibition efficiency of PASP on CaSO_4 .

3.3.2. X-ray diffraction (XRD) characterization

X-ray diffraction (XRD) is commonly used to analyze crystal properties (Li et al., 2019). The XRD patterns were identified with HighScore Plus software and the JCPDS library, which identified the phase of the scale. To explore the effect of PASP/8AC on the formation of calcium scale crystals, the phases of the crystals formed in the presence and absence of inhibitors were observed with diffraction analyses. The XRD patterns of the CaSO_4 and CaCO_3 scales are exhibited in Fig. 6a and 6b, respectively.

Compared with the peaks in the XRD pattern of CaSO_4 scale formed without the inhibitors, the peaks became weaker and wider with PASP or PASP/8AC (Fig. 6a). The literature shows that weak diffraction peaks mean lower crystallinity of the sample, and the layers were more separated. Compared with the narrower peaks, the wider peaks reflected smaller crystalline particles (Liang, 2023). These results indicated that the addition of PASP and PASP/8AC did not change the composition of CaSO_4 crystals, but inhibited the formation of CaSO_4 scale and produced a lattice distortion effect, resulting in smaller particles and thus lower crystallinity. PASP/8AC contains many functional groups, such as $-\text{COOH}$, $-\text{OH}$ and $\text{C}=\text{O}$, which were adsorbed on the crystal surfaces. It is hypothesised that, in addition to the chelating effect of its own $-\text{COOH}$, the extended side-chain to side-chain, perhaps for some as yet unknown reason, is also involved in the formation of CaSO_4 crystals, affecting the growth of CaSO_4 crystals and resulting in smaller calcium CaSO_4 particles.

Fig. 6b shows that the CaCO_3 scale formed without inhibitor was mainly calcite. The 2θ peaks in the XRD pattern occurred at 23.045° , 29.526° , 34.974° , 44.165° , 49.813° and 57.442° , which correspond to the JCPDS data for calcite (-). After the addition of 50 mg/L PASP, although calcite was still the main morphology of the CaCO_3 scale, it is obvious that some calcite had been transformed into vaterite (\blacktriangle) based on the peaks at 31.152° , 37.889° , 41.263° , and 50.252° for vaterite. When 50 mg/L PASP/8AC was present, the data showed that vaterite generated peaks at 2θ values of 24.376° , 31.124° , 36.173° , 40.985° , 44.968° , 48.455° , 50.162° , 59.351° , and 60.247° . These results were consistent with the SEM surface morphologies of the CaCO_3 scale, indicating that the CaCO_3 scale was mainly composed of calcite crystals, and the crystals generated with the PASP inhibitor were mainly vaterite with a small amount of calcite. However, the CaCO_3 scale formed with the PASP/8AC inhibitor was basically vaterite. Calcite is the most stable form of CaCO_3 scale, and it is difficult to remove when formed and deposited in pipes. Vaterite is a soft scale that is relatively easy to clean when attached to the inner walls of a pipe. Both PASP and PASP/8AC can transform scale from hard scale to soft scale, but PASP/8AC had the better effect. It may be that the PASP/8AC carrying more carboxyl groups slowed the rate of crystal growth and hindered the growth more effectively.

3.3.3. XPS characterization

To confirm the scale inhibition effects of PASP and PASP/8AC, X-ray photoelectron spectroscopy (XPS) was applied to the CaCO_3 and CaSO_4

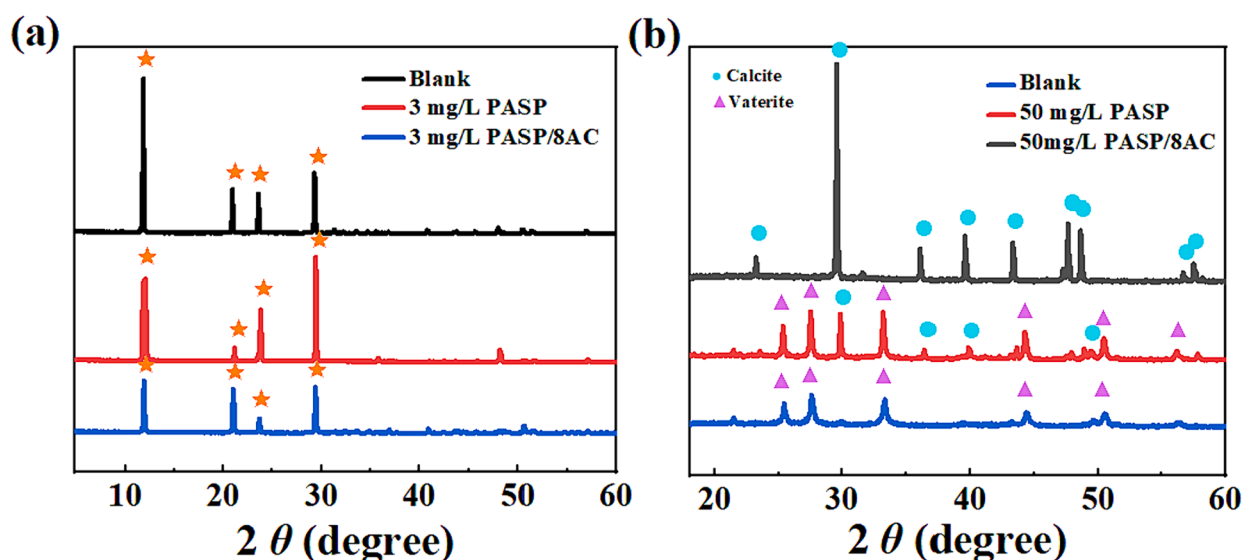


Fig. 6. XRD patterns of scale; (a) CaSO_4 scale sample, (b) CaCO_3 scale sample.

scales formed during the static scale inhibition tests, and the high-resolution Ca 2p XPS data for the CaCO₃ and CaSO₄ scales formed without and with the scale inhibitors are shown in Fig. 7 and Fig. 8. When the scale inhibitor was absent, the Ca 2p_{1/2} and Ca 2p_{3/2} peaks for the CaCO₃ scale were at 347.62 eV and 343.94 eV, respectively (Fig. 7). When 50 mg/L PASP was added, the Ca 2p_{1/2} and Ca 2p_{3/2} binding energies decreased by 0.28 eV and 0.30 eV, respectively. After the addition of 50 mg/L PASP/8AC, the Ca 2p_{1/2} binding energies increased by 0.10 eV, and the Ca 2p_{3/2} binding energies decreased by 0.79 eV. These results showed that PASP or PASP/8AC affected the chemical environments around Ca²⁺ ions, changed the crystal type of the CaCO₃, and then participated in the formation of CaCO₃ crystals. Compared with PASP, the change caused by PASP/8AC were more obvious.

Similarly, the Ca 2p peaks for the CaSO₄ scale were also shifted by the addition of PASP or PASP/8AC (Fig. 8). The difference was that the addition of PASP or PASP/8AC resulted in 0.16 eV and 0.62 eV increases in the Ca 2p_{1/2} binding energies, respectively. The Ca 2p_{3/2} binding energies were increased by 0.18 eV with the addition of PASP, and the Ca 2p_{3/2} binding energies were decreased by 0.36 eV. These results showed that the electronegative groups in PASP and PASP/8AC bound Ca²⁺, which prevented the formation and growth of crystal nuclei for the CaSO₄ scale and delayed the formation of scale in the aqueous solution. In addition, because PASP/8AC contained longer side chains and more -COOH groups, it had a higher Ca²⁺-binding capacity than PASP.

3.4. Scale inhibition mechanism

3.4.1. Induction time measurements of CaCO₃ scale

The nucleation induction time (t_{ind}) is an important parameter used to measure the properties of CaCO₃ solutions, which reflects the rate and sizes of CaCO₃ crystal nuclei formation. Therefore, to study the scale inhibition mechanism, the t_{ind} values of CaCO₃ solutions with four different supersaturated concentrations (0.015 mol/L, 0.020 mol/L, 0.025 mol/L, 0.030 mol/L) in the presence and absence of agents were observed, as shown in Fig. 9 and Table 2. The supersaturated solution of CaCO₃ was prepared by adjusting the ratio of Ca²⁺ ions to CO₃²⁻ ions. As shown in Table 2, with increases in the CaCO₃ supersaturation ratio in the absence of inhibitor, the scale formation rate decreased, which was consistent with classical nucleation theory. The nucleation time of CaCO₃ was prolonged to some extent by addition of the PASP inhibitor. However, addition of the PASP/8AC inhibitor greatly extended the t_{ind} of the CaCO₃ crystals. Compared with the blank control, when the concentration of CaCO₃ solution was 0.015 mol/L, the nucleation induction time was extended from 1.5 min to 151.13 min, and even when the concentration was 0.03 mol/L, the nucleation induction time was extended by 14.9 min. These results were consistent with the SEM results above. Both the elongated chains and the increased number of carboxyl groups in the PASP/8AC polymer improved its ability to bond with Ca²⁺ ions, reduced the local supersaturation, and inhibited the formation of crystal nuclei.

In addition, according to the t_{ind} values, the surface energies of CaCO₃ in the presence and absence of scale inhibitors were calculated with Formula 2. The surface energy of CaCO₃ in the absence of a scale inhibitor was 39.6 mJ·m⁻². After addition of the PASP and the PASP/8AC scale inhibitors, the surface energies of CaCO₃ were 45.1 mJ·m⁻² and 50.9 mJ·m⁻², respectively. The increased surface energy was due to additional interactions among the cations, scale inhibitors and micro-crystals, which reduced the nucleation rate of the calcium carbonate crystals and delayed agglomeration of the crystals. Compared with PASP, the surface energy of CaCO₃ was only increased by 5 mJ·m⁻² in the presence of PASP/8AC. Combined with the nucleation induction time t_{ind} , these results suggested that PASP/8AC did not interfere with the formation of CaCO₃ scale through typical lattice distortion. Along these lines, we speculated that PASP/8AC reduced the binding rate of Ca²⁺ ions and CO₃²⁻ ions mainly through chelation of the Ca²⁺ ions. Another possibility is that although both PASP and PASP/8AC were adsorbed on the CaCO₃ surface, PASP/8AC was more likely to bind to the active sites of Ca²⁺ ions, thus inhibiting the growth of CaCO₃ crystals.

3.4.2. Optimization of the PASP/8AC structure

To deeply unravel the scale inhibition mechanism of PASP/8AC polymer, the optimized structure and Mulliken charge distribution of PASP/8AC based on quantum chemistry calculations are conducted and exhibited in Fig. 10 and Table 3, respectively. The electronegativities of the atoms are key factors in chemical reactions, affecting the ability to interact with other atoms and the structures of molecules, which in turn affect the stabilities and solubilities of molecules. The two N atoms in PASP/8AC carried negative charges of -0.670205 and -0.56224, and the four O atoms had negative charges of -0.36739, -0.38665, -0.43108 and -0.5643. The highly negative charges of the N and O atoms meant that more sites were available to bind more Ca²⁺ ions, which in turn hindered the growth of CaCO₃ crystals and inhibited the formation of calcium scale. In addition, the compounds formed by atoms with greater electronegativity combined with ions have higher stabilities. During long-term operation of industrial circulating water, large amounts of calcium scale are formed and attached to the pipe walls, reducing the heat transfer efficiency of the pipeline and so on. After adding the PAPS/8AC scale inhibitor with many NH₂ and -COOH groups on the longer side chains, it combined with the positively charged calcium ions, reduced the concentration of Ca²⁺ ions, and restrained the generation of calcium scale. PASP/8AC contains many negatively charged nitrogen and oxygen atoms, which combined with calcium ions to form a stable and soluble substance that was not easily deposited. Therefore, the PASP/8AC scale inhibitor controlled the deposition of calcium scale, which provides a basis for the development of green and efficient water treatment chemicals.

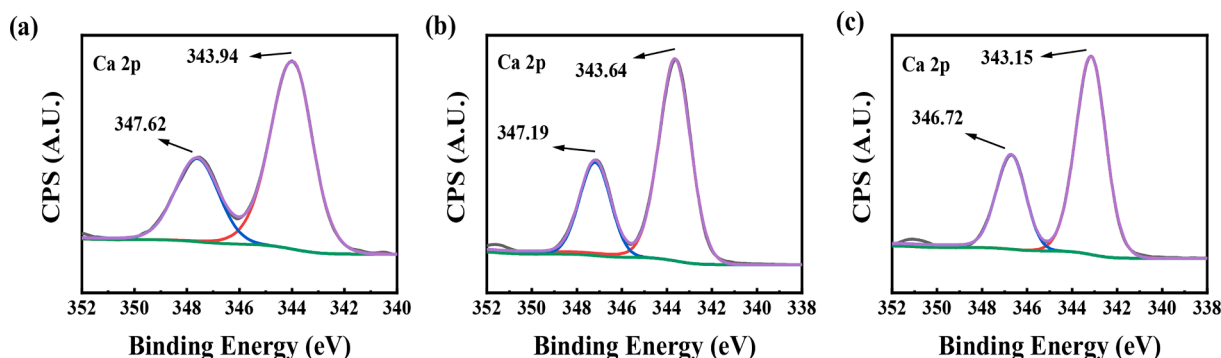


Fig. 7. Ca 2p XPS spectra of CaCO₃ scales; (a) without the scale inhibitor, (b) with 50 mg/L PASP, (c) with 50 mg/L PASP/8AC.

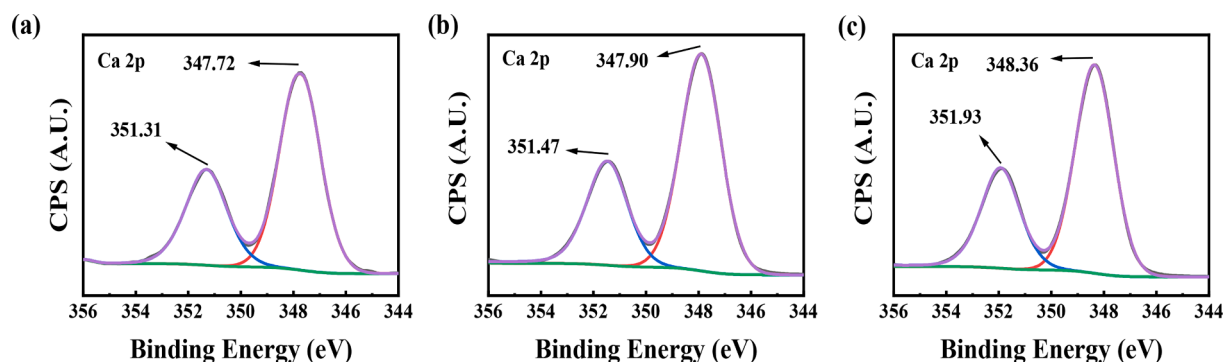


Fig. 8. Ca 2p XPS spectra of CaSO_4 scales; (a) without the scale inhibitor, (b) with 3 mg/L PASP, (c) with 3 mg/L PASP/8AC.

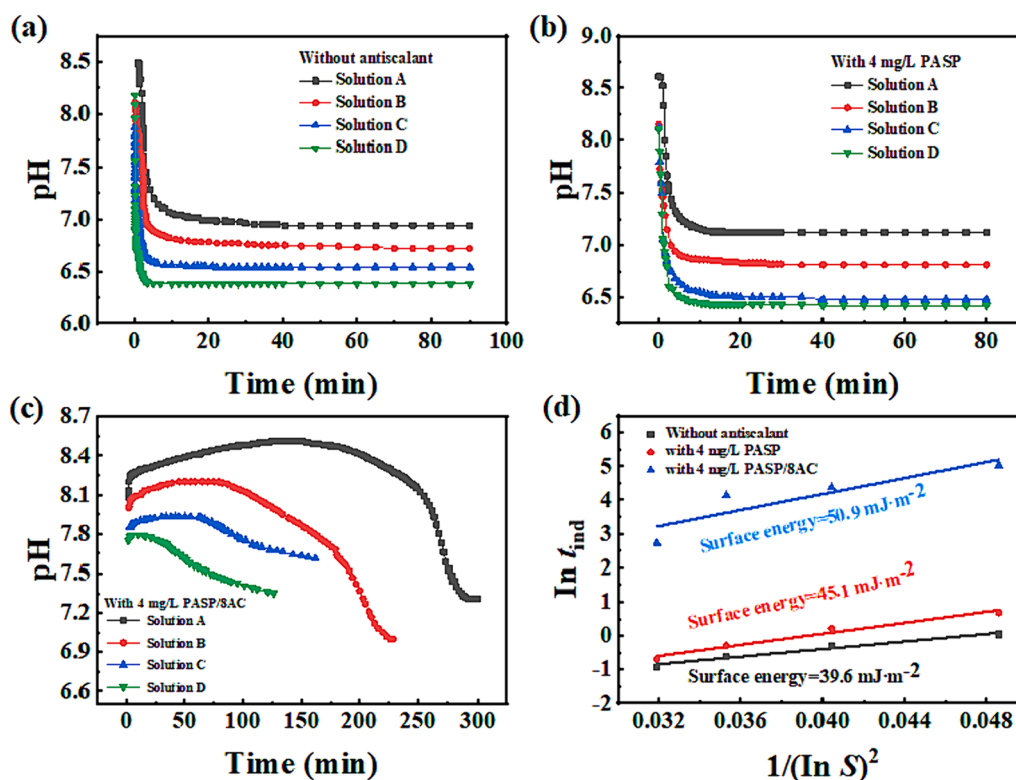


Fig. 9. The relationship between $\ln t_{\text{ind}}$ and $1/(\ln S)^2$ without inhibitor, with 4 mg/L PASP and 4 mg/L PASP/8AC.

Table 2

The t_{ind} of CaCO_3 solution without antiscalant and in the presence of PASP and PASP/8AC.

	Inhibitors	CaCO ₃ solutions with different concentrations (mol/L)			
		0.015	0.020	0.0250	0.030
t_{ind} (min)	Blank	1.50	0.75	0.54	0.40
	PASP	2.25	1.25	0.75	0.50
	PASP/8AC	151.13	79.08	62.2	15.3

4. Conclusions

A new scale inhibitor, the 8-aminocaprylic acid-modified PASP derivative (named PASP/8AC), was synthesized by open loop modification with polysuccinimide (PSI) and 8-aminooctanoic acid (8AC). The static scale inhibition test results showed that when the concentration of PASP/8AC was 3 mg/L, the scale inhibition efficiency of CaSO_4 was close to 100%. The scale inhibition efficiency of CaCO_3 was increased by

36% at a dosage of 5 mg/L. Moreover, compared with PASP, PASP/8AC had better thermal stability.

Mechanistic studies showed that PASP/8AC carried more O and N atoms with negative charges, which interacted with the Ca^{2+} ions and then participated in the formation of calcium scale, changed the crystal shapes of the calcium scale, and inhibited or delayed the formation of calcium scale. In addition, due to the longer PASP/8AC side chains, after interacting with Ca^{2+} , a three-dimensional NBO-type structure was formed to improve the heat resistance and scale inhibition efficiency, which provides a new idea for research and development on new water treatment agents.

Data availability

Data generated and analyzed during this study are included in the present paper. The raw datasets that support the findings of this study are available from the corresponding author upon reasonable request.

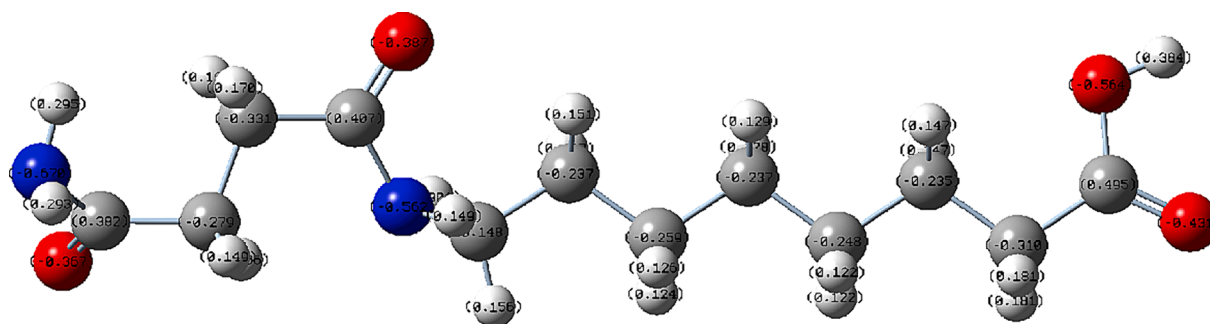


Fig. 10. Optimized structure of PASP/8AC.

Table 3

Mulliken charge distribution of PASP/8AC.

Mulliken atomic charges:			Mulliken atomic charges:		
1	N	-0.670205	21	H	0.12747
2	H	0.295478	22	C	-0.25863
3	H	0.29332	23	H	0.125689
4	C	0.382345	24	H	0.123778
5	O	-0.36739	25	C	-0.2373
6	C	-0.27909	26	H	0.128747
7	H	0.148818	27	H	0.127568
8	H	0.206325	28	C	-0.24846
9	C	-0.33143	29	H	0.122168
10	H	0.170051	30	H	0.122298
11	H	0.1927	31	C	-0.23549
12	C	0.407296	32	H	0.146723
13	O	-0.38665	33	H	0.146814
14	N	-0.56224	34	C	-0.30957
15	H	0.301002	35	H	0.180929
16	C	-0.1479	36	H	0.181125
17	H	0.156347	37	C	0.494755
18	H	0.149185	38	O	-0.43108
19	C	-0.23699	39	O	-0.5643
20	H	0.151286	40	H	0.384494

CRedit authorship contribution statement

Linlin Zhao: Data curation, Writing – original draft. **Fei Wang:** Resources, Project administration. **Xiaojuan Zhang:** Methodology. **Yu Han:** Investigation. **Yuxia Wang:** Investigation. **Zhenli Yang:** Project administration. **Zhongyan Cao:** Data curation. **Yufeng Wu:** Project administration. **Ying Xu:** Writing – review & editing.

Declaration of competing interest

The authors declare that they have no known competing financial interests or personal relationships that could have appeared to influence the work reported in this paper.

Acknowledgements

This study was funded by National Major Research and Development Plan Project (SQ2020YFF0402903). Thanks to Springer Nature Author Services for providing us with article language services.

References

- Ali, S.A., Kazi, I.W., Rahman, F., 2015. Synthesis and evaluation of phosphate-free antiscalants to control $\text{CaSO}_4 \cdot 2\text{H}_2\text{O}$ scale formation in reverse osmosis desalination plants. *Desalination* 357, 36–44. <https://doi.org/10.1016/j.desal.2014.11.006>.
- Ansari, K.R., Dheeraj, S.C., Sorour, A.A., et al., 2023. Experimental and computational approach on the development of a new green corrosion inhibitor formulation for N80 steel in 20% formic acid. *J. Colloid Interface Sci.* 652 (Pt B), 2085–2097. <https://doi.org/10.1016/j.jcis.2023.08.190>.
- Cai, Y.H., Zhao, J.L., Guo, X.Y., et al., 2022. Synthesis of polyaspartic acid-capped 2-aminoethylamino acid as a green water treatment agent and study of its inhibition

- performance and mechanism for calcium scales. *RSC Adv.* 12, 24596–24606. <https://doi.org/10.1039/d2ra04075a>.
- Chen J.X., Chen F.J., Han J., et al., 2020. et al, Evaluation of scale and corrosion inhibition of modified polyaspartic acid. *Chem Eng Technol* 6, 1048–1058. [10.1002/ceat.201900518](https://doi.org/10.1002/ceat.201900518).
- Chien, W.C., Tai, C.Y., Hsu, J.P., 1999. The induction period of the $\text{CaCl}_2\text{-Na}_2\text{CO}_3$ system: theory and experiment. *J. Chem. Phys.* 111, 2657–2664. <https://doi.org/10.1063/1.479541>.
- Čožíková, D., Šílová, T., Moravcová, V., 2017. Preparation and extensive characterization of hyaluronan with narrow molecular weight distribution. *Carbohydr Polym* 160, 134–142. <https://doi.org/10.1016/j.carbpol.2016.12.045>.
- Du, Q., Wang, Y.W., Li, A.M., et al., 2018. Scale-inhibition and flocculation dual-functionality of poly(acrylic acid) grafted starch. *J. Environ. Manage.* 210, 273–279. <https://doi.org/10.1016/j.jenvman.2018.01.016>.
- Eichinger, S., Boch, R., Leis, A., 2022. Green inhibitors reduce unwanted calcium carbonate precipitation: implications for technical settings. *Water Res.* 208, 117850. <https://doi.org/10.1016/j.watres.2021.117850>.
- Giuseppe, M.D.C., Prisciandaro, M., Karatza, D., et al., 2017. Salt scales on process equipment: measurement of the induction time for calcium carbonate nucleation. *Can J. Chem. Eng.* 9999, 1–5. <https://doi.org/10.1002/cjce.22878>.
- Glibert, P.M., 2017. Eutrophication, harmful algae and biodiversity - challenging paradigms in a world of complex nutrient changes. *Mar. Pollut. Bull.* 124, 591–606. <https://doi.org/10.1016/j.marpolbul.2017.04.027>.
- Ji, Y., Chen, Y., Le, J.X., et al., 2017. Highly effective scale inhibition performance of amino trimethylenephosphonic acid on calcium carbonate. *Desalination* 422, 165–173. <https://doi.org/10.1016/j.desal.2017.08.027>.
- Khormali, A., Sharifov, A.R., Torba, D.I., et al., 2018. Increasing efficiency of calcium sulfate scale prevention using a new mixture of phosphonate scale inhibitors during waterflooding. *J. Pet. Sci. Eng.* 164, 245–258. <https://doi.org/10.1016/j.petrol.2018.01.055>.
- Li, D.Z., Shao, H.L., Yang, F.M., et al., 2023. Fluorescent and antibacterial sulfur quantum dots as calcium sulfate scale inhibitor. *Desalination* 555, 116547. <https://doi.org/10.1016/j.desal.2023.116547>.
- Li, L., Wang, Y., Sun, Y., et al., 2021. Novel and green hydroxyperylene imide based fluorescent polymer for calcium sulfate scale inhibition. *J. Mol. Liq.* 344, 117730. <https://doi.org/10.1016/j.molliq.2021.117730>.
- Li, C., Zhang, C., Zhang, W., 2019. The inhibition effect mechanisms of four scale inhibitors on the formation and crystal growth of CaCO_3 in solution. *Sci. Rep.* 9, 13366. <https://doi.org/10.1038/s41598-019-50012-7>.
- Liang, J.K., 2023. Powder diffraction determination of crystal structure: advanced textbook. Chian Science Publishing & Media Ltd.
- Lin, L., Jiang, W.B., Xu, X.S., et al., 2020. A critical review of the application of electromagnetic fields for scaling control in water systems: mechanisms, characterization, and operation. *npj Clean Water* 3, 25. <https://doi.org/10.1038/s41545-020-0071-9>.
- Liu, X.H., Gao, Y.H., Gao, Y.J., et al., 2023. Synthesis of polyaspartic acid-glycidyl adduct and evaluation of its scale inhibition performance and corrosion inhibition capacity for Q235 steel applications. *Arab. J. Chem.* 16, 104515. <https://doi.org/10.1016/j.arabjc.2022.104515>.
- Liu, Z.Y., Sun, Y.H., Zhou, X.H., 2011. Synthesis and scale inhibitor performance of polyaspartic acid. *J Environ Sci-China* 23 (Supplement), S153–S155. [https://doi.org/10.1016/S1001-0742\(11\)61100-5](https://doi.org/10.1016/S1001-0742(11)61100-5).
- Nakanishi, M., Park, J.S., Jang, W.D., et al., 2007. Study of the quantitative aminolysis reaction of poly(β -benzyl L-aspartate) (PBLA) as a platform polymer for functionality materials. *React. Funct. Polym.* 67, 1361–1372. <https://doi.org/10.1016/j.reactfunctpolym.2007.08.009>.
- Nayunigari, M.K., Gupta, S.K., Kokkarachedu, V., et al., 2014. Development of anti-scale poly(aspartic acid-citric acid) dual polymer systems for water treatment. *Environ. Technol.* 23, 2903–2909. <https://doi.org/10.1080/09593330.2014.925510>.
- Piyadasa, C., Ridgway, H.F., Yeager, T.R., et al., 2017. The application of electromagnetic fields to the control of the scaling and biofouling of reverse osmosis membranes-a review. *Desalination* 418, 19–34. <https://doi.org/10.1016/j.desal.2017.05.017>.
- Qiang, Y., Guo, L., Li, H., et al., 2021. Fabrication of environmentally friendly losartan potassium flm for corrosion inhibition of mild steel in HCl medium. *Chem. Eng. J.* 406, 126863. <https://doi.org/10.1016/j.cej.2020.126863>.

- Rbaa, M., Fardioui, M., Verma, C., et al., 2020. 8-hydroxyquinoline based chitosan derived carbohydrate polymer as biodegradable and sustainable acid corrosion inhibitor for mild steel: experimental and computational analyses. *Int. J. Biol. Macromol.* 155, 645–655. <https://doi.org/10.1016/j.ijbiomac.2020.03.200>.
- Stamatakis, E., Stubos, A., Palyvos, J., et al., 2005. An improved predictive correlation for the induction time of CaCO₃ scale formation during flow in porous media. *J. Colloid Interf. Sci.* 286, 7–13. <https://doi.org/10.1016/j.jcis.2004.12.040>.
- Syeda, H.I., Muthukumar, S., Baskaran, K., 2023. Polyglutamic acid and its derivatives as multi-functional biopolymers for the removal of heavy metals from water: a review. *J. Water Process Eng.* 56, 104367. <https://doi.org/10.1016/j.jwpe.2023.104367>.
- Uchida, H., Miyata, K., Oba, M., et al., 2011. Odd-even effect of repeating aminoethylene units in the side chain of N-substituted polyaspartamides on gene transfection profiles. *J. Am. Chem. Soc.* 133, 15524–15532. <https://doi.org/10.1021/ja204466y>.
- Wallace, A.F., Hedges, L.O., Alejandro, F.M., et al., 2013. Microscopic evidence for liquid-liquid separation in supersaturated CaCO₃ solutions. *Science* 341, 885–889. <https://doi.org/10.1126/science.1230915>.
- Wang, Z., He, J., Tao, Y., et al., 2003. Controlled chain branching by RAFT-based radical polymerization. *Macromolecules* 36, 7446–7452. <https://doi.org/10.1021/ma025673b>.
- Wang, Y., Zhang, H.Z., Wang, T.P., et al., 2023. Research on mechanisms and effects of microbial agent applied in scaling control of circulating cooling water. *Int. Biodeter. Biodegr.* 185, 105682. <https://doi.org/10.1016/j.ibiod.2023.105682>.
- Whitfield, R., Truong, N.P., Anastasaki, A., 2021. Precise control of both dispersity and molecular weight distribution shape by polymer blending. *Angew. Chem. Int. Ed.* 60, 19383–19388. <https://doi.org/10.1002/anie.202106729>.
- Xiang, L., Ryu, W., Kim, H., et al., 2018. Precise synthesis, properties, and structures of cyclic poly(ϵ -caprolactone)s. *Polymer* 10, 577. <https://doi.org/10.3390/polym10060577>.
- Yan, M.F., Tan, Q.Q., Liu, Z., et al., 2020. Synthesis and application of a phosphorous-free and non-nitrogen polymer as an environmentally friendly scale inhibition and dispersion agent in simulated cooling water systems. *ACS Omega* 5, 15487–15494. <https://doi.org/10.1021/acsomega.0c01620>.
- Younes, I., Rinaudo, M., et al., 2015. Chitin and chitosan preparation from marine sources. structure, properties and applications. *Mar. Drugs* 13, 1133–1174. <https://doi.org/10.3390/md13031133>.
- Zeino, A., Abdulazeez, I., Khaled, M., et al., 2018. Mechanistic study of polyaspartic acid (PASP) as eco-friendly corrosion inhibitor on mild steel in 3% NaCl aerated solution. *J. Mol. Liq.* 250, 50–62. <https://doi.org/10.1016/j.molliq.2017.11.160>.
- Zhang, S.P., Qu, H.J., Yang, Z., et al., 2017. Scale inhibition performance and mechanism of sulfamic/amino acids modified polyaspartic acid against calcium sulfate. *Desalination* 419, 152–159. <https://doi.org/10.1016/j.desal.2017.06.016>.
- Zhang, M.L., Ruan, Z., Han, Y., et al., 2024. Controllable synthesis of polyaspartic acid: studying into the chain length effect for calcium scale inhibition. *Desalination* 570, 117080. <https://doi.org/10.1016/j.desal.2023.117080>.
- Zhao, J.L., Zhang, M.L., Zhang, Z.K., et al., 2022. Polyaspartic acid-capped 4-[(2-aminoethyl) amino]-4-oxobutanoic acid as an efficient and green gypsum scale inhibitor and its scale inhibition mechanism. *Desalination* 543, 116101. <https://doi.org/10.1016/j.desal.2022.116101>.
- Zhao, L.N., Zhou, Y.M., Yao, Q.Z., et al., 2021. Calcium scale inhibition of stimulated oilfield produced water using polyaspartic acid/aminomethanesulfonic acid. *ChemistrySelect* 6, 3692–3701. <https://doi.org/10.1002/slct.202100853>.